Integrative Genomic Analysis of In-Vivo Muscle Regeneration After Severe Trauma

Carlos A. Aguilar[1,*], Anna Shcherbina[1], Ramona Pop[2], Ronald W. Matheny[3], Davide Cacchiarelli[2], Christopher T. Carrigan[3], Casey A. Gifford[2], Melissa A. Kottke[3], Darrell O. Ricke[1], Maria L. Urso[3,†], Alexander Meissner[2]

[1]Massachusetts Institute of Technology - Lincoln Laboratory, Lexington, MA 02127. [2]Broad Institute of MIT and Harvard, Cambridge, MA 02142, Harvard Stem Cell Institute, Cambridge, MA 02138, Dept. of Stem Cell and Regenerative Biology, Harvard University, Cambridge, MA 02138. [3]United States Army Institute of Environmental Medicine - Military Performance Division, Natick, MA 01760. [†]Present address: Smith and Nephew, Biotherapeutics, Ft. Worth, TX, 76132.

*To whom correspondence should be addressed: carlos.aguilar@ll.mit.edu

Abstract: Adult skeletal muscle is the dominant system through which complex physical actions are accomplished and is uniquely capable of repair and regeneration after different types of insult or injury via resident stem cells. The *in-vivo* epigenomic and transcriptional mechanisms through which skeletal muscle repairs itself are partly understood and herein, we administer severe muscle trauma to a mouse tibialis anterior muscle and monitor the *in-vivo* dynamics of three histone modifications and gene expression across nine time points after injury. Integrating the genome-wide datasets, we show extensive chromatin state remodeling at *cis*-regulatory elements and observe the cooperative activity of lineage-specific transcription factors during progressions through different stages of healing. We highlight how one of the major regenerative programs (IGF and PI3K signaling) activated after injury is titrated by negative regulators temporally on multiple levels. Lastly, we illustrate the dynamics of non-coding RNAs during various stages after trauma, most notably during the switch from myoblast proliferation towards differentiation and eventual muscle regeneration. These results provide an unbiased, comprehensive view of the central factors that regulate muscle regeneration after severe trauma and underscore the multiple levels through which both local and global genetic and epigenetic patterns are regulated to enact appropriate and timely repair and regeneration.

Introduction

Adult skeletal muscle is a post-mitotic organ that coordinates movement and constantly grows and adapts by remodeling its structure and metabolism. After insult or injury, adult skeletal muscle enables repair and regeneration of existing fibers through a population of stem cells that reside underneath the basal lamina called satellite cells[1] (SCs). The SCs reside in a specialized *niche*[2,3] and change their quiescent complexion after injury via various environmental signals and communication with infiltrating immune cells[4,5] and fibro-adipocyte progenitors (FAPs)[6]. Many essential SC regulators have been studied during the muscle repair and regeneration process, providing an excellent model to study the actions of different factors that support myogenic repair and regeneration sub-processes.

It is well established that multiple repair and regeneration sub-processes accomplished by SCs (and other cell types) after muscle injury are orchestrated by distinct transcriptional networks[7], encompassing epigenetic[8,9], transcriptional[10] and post-transcriptional events. However, the integrative dynamics of transcriptional networks and regulatory epigenetic switches at genome-wide levels have not been characterized in-vivo and as such, our understanding of the molecular processes and transcription factors (TFs) involved in myogenesis and muscle regeneration have been limited. Profiling the expression and chromatin state of *cis*-regulatory elements[11] after severe muscle trauma provides a powerful method to understand the molecular determinants of cellular fate, healing progression after severe muscle trauma and can provide crucial insights for development of therapeutic modalities for effective repair and regeneration of severe muscle trauma, myopathies such as Duchenne muscular dystrophy and aging.

The *cis*-regulatory networks that orchestrate *in-vivo* muscle repair and regeneration after traumatic injury have only been partly characterized[12,13] and herein, the dynamic *in-vivo* evolution of expression and three different chromatin modifications (H3K4me3, H3K4me1 and H3K27ac) were profiled across nine time points (t = 3 hrs to 672 hrs) from an injured and uninjured contralateral tibialis anterior muscle. The generated genomic maps were then contrasted against MyoD and MyoG ChIP-seq data from C2C12 cells[14,15] to determine shared and distinguishing signatures at *cis*-regulatory elements during different stages after injury. The dynamic chromatin state transitions, differential binding at TF motifs, levels of numerous coding and noncoding transcripts and corresponding adaptive molecular responses were integrated and assessed to construct a comprehensive view of the key transcriptional and chromatin factors that influence and modulate *in-vivo* muscle repair and regeneration dynamics.

Results

Severe muscle trauma induces extensive transcriptional changes and chromatin state remodeling

Figure 1 shows chromatin immunoprecipitation followed by DNA sequencing (ChIP-Seq) was used to globally map the chromatin state of various *cis*-regulatory elements at nine time points that were lumped into three key stages after a traumatic muscle injury (early: 3-24 hours after injury, middle: 48-168 hours after injury, late: 336-672 hours after injury). Validated antibodies (Supp. Fig. 1) for histone H3 lysine 4 trimethylation (H3K4me3), a modification associated with promoters, H3K4me1 and H3K27ac, associated with poised and active enhancer regions[16], respectively, were used to enrich chromatin. Each tissue from each time point was immuno-precipitated using the three antibodies, and ChIP-Seq maps from the same antibody and time point were merged, resulting in 54 chromatin-state maps covering >1.5 billion reads. RNA-Seq

maps for both the injured and contralateral tissues for each time point were also generated and analyzed[17]. Hierarchical clustering of the RNA-Seq data through time and peak fold change revealed clusters upregulated at different time periods that were associated with different stages of muscle repair and regeneration (Fig. 1b). Chemokine ligands CCL2 and CCL7, which are important for the recruitment of various immune cells to the injured muscle, peaked in expression in the early period (at 24 h after injury). Annexins 1 and 2 (Anxa1 and Anxa2), cellular membrane binding proteins, demonstrated a different expression profile and peaked in the middle period (between 48h and 72h) after injury suggesting the beginning of the regenerative program. Tropomyosins 3 and 4 (Tpm3 and Tpm4), thin filament proteins that participate in muscle contraction, demonstrated a similar temporal expression profile to the annexin family and other sarcomere proteins, which peaked in the middle period and remained upregulated into the late stage, in line with a productive healing process.

Figure 2 shows in the early time period, 93,149 sites were enriched for H3K4me3, and 104,890 sites for the middle period followed by 141,948 sites for the late period. Of these, 1,606 were differentially enriched in the early time points relative to the controls, 6,733 in the middle time points, and 6,121 in the late time points (Supp. Fig. 2). To integrate sites that gained or lost the H3K4me3 modification during the time course with transcriptional activity (FPKM>1), RNA sequencing (RNA-Seq) results were performed at the same time points[17] and contrasted against the genome-wide maps. Approximately 58% percent of sites were found to associate with transcriptional activity (FPKM>1) and 4,241 sites exhibited dynamics (acquisition or loss of the histone modification) through at least one stage (early-middle, middle-late, early-late).

In contrast to H3K4me3, which has previously been shown to be largely static during chromatin remodeling events[18], H3K4me1 and H3K27ac demarcate enhancer elements, which are highly dynamic[19]. H3K4me1 resides on both poised and active enhancers, as to where H3K27ac marks active enhancers[20]. In the early time period, 93,938 sites enriched for H3K4me1 were identified, 106,353 sites for the middle period, and 28,663 sites for the late period. The active enhancer mark H3K27ac showed similar behavior with 32,285 sites enriched in the early time period, 43,780 sites in the middle period and 13,748 sites for the late period. Figure 2 depicts the highest number of sites that acquired H3K27Ac was found in the 72hr period (28,178 sites) compared to 11,535 for the 48hr stage and 4,067 for the 168hr stage.

Immune Cell Programs Contribute to Differential Chromatin States After Severe Trauma

In the early period, numerous transcripts associated with inflammation, invading immune cells[4], cytokine signaling, and apoptosis were detected. Gene Ontology (GO) term analysis of the enriched chromatin peaks in the early period that underwent changes for the injured samples relative to uninjured controls demonstrated enrichments similar to the transcriptional groups associated with immune response, chemokine and cytokine signaling, inflammation, and metabolism of lipids and lipoproteins (Fig. 3a & Supp. Fig. 3). The increase in number of enriched chromatin peaks associated with immune response and inflammatory pathways can partially be attributed to infiltration of monocytes, lymphocytes and macrophages, which are essential for functional recovery and generally follows a two-stage process. In the first stage, the invading immune cells induce a protective, pro-inflammatory state and after several days, switch to an anti-inflammatory program[5]. In line with this observation, transcription factor binding analysis of the enriched *cis*-regulatory sites showed binding motifs for cellular stress TFs such as NF-κβ, serum response factor (SRF), PU.1 and AP-1 (Fig. 2d), which promote chromatin accessibility and facilitate additional TFs to bind and modulate expression levels. The result of

these enrichments at *cis*-regulatory elements is also consistent with high expression of IL-6 and TNFα, both of which induce genes such as c-Fos, c-Jun, Atf1, Atf3 (Fig. 3c-d) and JunB (Supp. Fig. 3). Additional binding sites were also observed for STATs and JAK-STAT signaling, which along with pro-inflammatory cytokines activate downstream target genes such as c-Myc, reported to drive satellite cell proliferation[21] and repress myogenic TFs such as MyoD and MyoG (Supp. Fig. 4). These TF-coordinated programs most likely permit the injured site to activate and simultaneously titrate satellite cell expansion and immune cell infiltration as well as prevent premature myogenic differentiation.

Tissue Architecture Cues Influence Chromatin States & Transcription Factor Binding

In the middle time period (48-72hrs after injury), upregulation of SMADs and TGF-β signaling was observed along with increases in expression of TFs such as Tead4 and MyoD. These two elements act to repress c-Myc expression and promote a transition from proliferation and Notch signaling towards Hippo and Wnt signaling[22,23] (Fig. 4a). SMADs have been shown to interact with chromatin remodeling complexes such as histone acetyltransferases p300 and CBP (CREB-binding protein) to induce H3K27 acetylation, which is consistent with the observation that the highest number of sites that acquired H3K27ac was in the middle time period (Fig. 1d).

GO analysis of the differential H3K27ac peaks in the injured samples for the middle period revealed multiple enrichments for G-protein coupled receptors (Fig. 4b) and the Rho family of small GTPases. This result is consistent with the peak in expression of SRF target genes and anti-inflammatory cytokines interleukin-4 (IL-4) and interleukin-10 (IL-10), which induce M2 macrophage polarization and are essential components for resolution of inflammation and tissue repair[5] (Fig. 4a). Intriguingly, RhoA, GTPase and SRF each selectively modulate the expression of MyoD[24]. Increases in expression of these factors was also mirrored by upregulation of the macrophage-derived matrix metalloproteinase 12 (Mmp12), which cleaves and inactivates CXC chemokines (Cxcl1, -2, -3, -5, and -8) and monocyte chemotactic proteins (Ccl2, -7, -8, and -13), inhibiting leukocyte flux to the injured site and abrogating the amount of pro-inflammatory molecules present in the injured tissue (Supp. Fig. 4). Lastly, differential H3K27ac enrichments (Fig. 4c) were viewed for genes associated with extracellular matrix remodeling, such as components of the basement membrane (myoferlin, laminin, collagen VI genes, annexins), and alter the stiffness of newly formed or repaired ECM. Upregulation of GPCRs and altered ECM stiffness[25] have previously been shown to stimulate mechano-sensitive Yap and Taz to translocate into the nucleus and induce expression of genes that promote satellite cell proliferation[26], migration and Hippo and Wnt signaling.

The collective integration of these different enrichments at *cis*-regulatory elements for the middle period suggests the elastic nature of injured microenvironment (which is also regulated by invading fibroblasts and different types of immune cells) and anti-inflammatory soluble signals provide cues for nuclear shuttling of TFs[27] and activation of enhancers that signal the resident SC population to expand[28] and migrate towards damaged fibers. This result also implies that regenerating muscle possesses a plastic chromatin state at enhancers[29], which can provide flexibility to quickly respond to different ECM cues as well as facilitate sensitive interactions with invading cell types that may further influence differential usage of *cis*-regulatory elements.

Transcription Factor Coordinated Activation of Myogenic Differentiation and Regeneration

In the middle period, a unique and complex set of events occurs whereby multiple pathways begin the process of muscle repair and regeneration. Analysis of the total and differential

H3K27ac enrichments for the middle period revealed multiple binding sites for MyoD, MyoG and MEF2, along with RunX, Teads, PPARγ and various ternary complex factors (TCFs) of the ETS-domain family. At enriched promoter peaks for both the MyoD and MyoG datasets ($K4me3^+$ & $MyoD^+$ or $K4me3^+$ & $MyoG^+$), we also find binding motifs for Prdm14, a known histone methyltransferase, and Pbx3, a TF that cooperatively acts with MyoD to enact fast-twitch muscle expression[30]. Next, focusing on the enhancer sites ($H3K27ac^+$ & $H3K4me3^-$) during the middle period, the number of enriched sites that overlapped with MyoD binding was viewed to peak at 72hrs (Fig. 5a). This observation is consistent with the largest increase in sites that acquired H3K27ac was at 72h as well as the known association between MyoD and p300/CBP on E-box motifs of target genes during myogenic differentiation. The increase in detected MyoD binding sites at enhancers also mirrored the temporal activation of enriched GO terms associated with myogenic differentiation (Fig. 5c) such as different types of growth factor signaling (insulin growth factor – IGF, fibroblast growth factor – FGF, hedgehog), p38 mitogen-activated protein kinase (p38-MAPK), and phosphatidylinositol 3-kinase (PI3K) signaling (discussed further below). IGF signaling plays a crucial role in muscle repair and regeneration after injury and previous efforts have shown that activated satellite cells express IGF binding proteins (IGFBPs) [31]. Concordantly, several IGFBPs and IGF2 were observed to be upregulated in this time period (Fig. 5b). The p38 MAPK pathway has also previously been shown to stimulate myogenic transcription through recruitment of the chromatin-remodeling complex SWI-SNF to specific loci and neutralizes TFs such as c-Jun that inhibit cell-cycle exit[32]. In line with this, we view induction of cyclin-dependant kinase inhibitor p21, which is activated by MyoD and promotes cell-cycle exit and GSEA reactome sets associated with DNA unwinding. The presence of PPARγ enrichments may be derived from resident fibro/adipogenic progenitors that expand and proliferate in damaged muscle tissue to produce factors that support myogenic differentiation[6,33]. The various pathways converge to direct TFs such as MyoD, Myogenin (MyoG) and MEF2 towards various muscle-specific genes and promote myogenic differentiation. Intriguingly, during the middle period, enhancer sites associated with enriched MyoD or MyoG binding did not exhibit many overlapping enriched motifs. MyoG peaks at enhancers showed enrichment for multiple ETS-domain proteins, Teads, IRFs, MEF2a and Stats, which was in contrast to MyoD peaks at enhancers that showed enrichment for RunX, Pbx, p300, Meis1 and NF-κβ, which is modulated by the PI3k-Akt signaling pathway. Amalgamating these results suggests the onset of myoblast differentiation and myocyte formation and a unique cooperativity for different myogenic TFs (Fig. 5d).

Positive and Negative Regulation of Myogenic Differentiation Occurs on Cis and Trans Levels

Skeletal muscle regeneration is tightly regulated through a variety of positive and negative feedback regulatory pathways and an excellent example is through the IGF pathway, which serially activates PI3K, Akt and mammalian target of rapamycin (mTOR). Several of the effector kinases of these pathways (protein kinase B -Akt/PKB and extracellular-signal-regulated kinase 1/2 - ERK1/2) were shown in Figure 3b as key hubs within the transcriptional network orchestrating the early phase of repair and regenerative response. One component of the IGF pathway, the PI3K component, is essential for skeletal muscle regeneration; and the PI3K enzymes are heterodimers composed of a catalytic subunit bound to a regulatory subunit. Three Class IA PI3K p110 catalytic subunits (α, β, and δ) are expressed in skeletal muscle[34], and of these, p110α and p110β have been shown to positively influence myoblast proliferation and differentiation[35,36]. The single Class IB PI3K p110 catalytic subunit γ is expressed abundantly in immune cells, and association with Gβγ subunits mediates downstream signal transduction. In

the early and middle phases (24-72h) following injury (the period associated with peak myoblast proliferation), we observed differential enhancer binding and increases in expression of PI3K catalytic subunits p110α (*Pik3ca*), p110β (*Pik3cb*), and p110δ (*Pik3cd*) for the injured muscle as compared to the contralateral control. Figure 6 shows increases in expression and active enhancers of the PI3K p85α (*Pik3r1*) regulatory subunit along with increases in expression and chromatin remodeling of Class IB p110γ (*Pik3cg*) and its regulatory subunit p101 (*Pik3r5*) during the healing process.

The temporal increases in PI3K expression (and other positive myogenic regulatory pathways) between 24h-72h post-injury were also mirrored by chromatin changes and increases in expression of negative feedback regulators such as MG53 (Trim72[37], XBP1[38], USF1, Id1, Id2, NFATc1[39] and several HDACs), which associate with MyoD and MEF2 proteins to repress their activity[40]. The negative regulators began to decrease in expression starting at 72h, further reinforcing the observation of induction of myogenic differentiation at this time. Collectively, these observations suggest that the IGF, PI3K and AKT pathways crosstalk with negative regulators at different levels to direct competition, co-occupancy or occlusion of MyoD and MEF2 binding sites (XBP1, USF1), binding to MyoD and MEF2 to reduce their binding affinity (Id1, Id2, NFATc1, HDACs) as well as disrupting upstream IGF signaling via ubiquitin ligases (MG53) to precisely tune myogenic repair and regeneration programs.

Positive and negative regulation of muscle regeneration has also recently been shown to occur post-transcriptionally, where muscle-specific microRNAs (miR-1-a/133a-2, miR-1-b/133a-1, miR206/133b) bind to the 3′ untranslated region (UTR) of mRNAs that promote or repress myogenic gene expression programs and inhibit translation[41,42]. Small RNA-Seq was performed at multiple time points from each stage (early: 3h & 10h; middle: 72h, 168h, 336h; late: 504h, 672h) to probe *trans*-regulation of muscle regeneration dynamics and 841 miRNAs were detected for at least one time point and of these, 143 miRNAs showed dynamic behavior (See Methods). Figure 7a shows the results of the small RNA-Seq data and examination of muscle-specific microRNAs revealed changes in expression in the middle and late periods (downregulation of miR-133a and miR-1b, upregulation of miR-206, miR-133b and miR-1a), which is consistent with the temporal upregulation of their regulatory factors MyoD and MyoG and chromatin profiles exhibiting active enhancer activity (Fig. 7b)[43]. Further analysis of the datasets reinforced many of the results observed from the RNA-Seq and ChIP-Seq datasets, where early upregulated microRNAs were associated with inflammation and immune system programs and middle and late stage upregulated microRNAs were associated with muscle repair and regeneration. For example, in the early period the inflammatory miR-223 was upregulated as to where its expression subsided in the middle and late periods. In the middle period, when the nascent stage of myogenic differentiation was observed, upregulation of miR126b (associated with angiogenic and chemokine signaling[44]), and miR-429 (transcriptional repressor of c-myc and proliferation), was detected. Additionally, several other miRs linked to skeletal muscle regeneration[45,46] exhibited changes in expression during the middle period such as the miR-29 family (regulator of fibrosis and collagen expression), miR-21 (regulator of PI3k/Akt signaling), miR-31 and as well as the miR378 cluster (regulator of mitochondrial metabolism and inhibitor of musculin). The delicate balances in expression of these *trans*-regulatory elements through time are uniquely further titrated by competing endogenous RNAs (ceRNAs) such as linc-MD1[47], which sequesters transcripts such as miR133 to facilitate myogenic differentiation transcriptional programs. Figure 7c demonstrates the temporal expression profile of linc-MD1,

which was dramatically upregulated beginning at 72h and peaked at 168h, consistent with the peak times observed for myoblast proliferation and onset of differentiation.

Discussion

Muscle recovery after traumatic injuries such as an occupational crush or blast suffered during military combat canonically induces a predisposition for additional injuries and chronic pain. Many of the various muscle repair and regeneration sub-processes triggered after trauma have been studied and shown to be orchestrated by gene expression networks controlled by lineage-specific TFs such as MyoD, MyoG, and MEF2. However, many questions at the molecular level remain and the *in-vivo* epigenomic landscape after trauma has not been fully characterized and as such, our understanding of how these different factors translate to influence the chromatin architecture that regulates expression at lineage-specific genes has been limited. Herein, we use integrative genomic mapping technologies to profile the *in-vivo* chromatin state of various *cis*-regulatory elements and gene expression and found successive waves of chromatin remodeling orchestrated by combinations of lineage-specific TFs.

The ChIP-Seq maps revealed *cis*-regulatory elements such as promoters were largely invariant when compared to regions demarcated by enhancer marks (H3K4me1, H3K27ac), which demonstrated dynamic behavior. The motifs enriched within H3K27ac regions immediately after the injury until 48-72h later were associated with canonical mediators of early stress, immunity and growth factor responses such as AP-1 (Fos/Jun), SRF, NF-κβ, EGR, and STATs. A significant fraction of the TF binding sites correlated with transcriptional dynamics and was most likely attributable to infiltrating monocytes that secrete and respond to cytokines and chemokines. These early immune-related changes were paralleled by pathways associated with activation and proliferation of satellite cells, such as Notch, Hippo and TGF-β signaling. Three days after the injury, the epigenetic landscape changed and could be attributed to proliferating satellite cells that began the process of myogenic differentiation. These changes were orchestrated through concerted binding of TFs such as MEF2, MyoD, MyoG, Teads, RunX, Pbx and PPARγ and chromatin regulators[48] such as p300, CBP and SWI/SNF. In contrast to the early period, which was dominated by interactions with invading immune cells, the middle and late periods were enriched for TF-binding sites that were associated with structural genes, cellular migration and niche remodeling. The two different types of interactions offer a unique insight into how the plastic chromatin state of regenerating muscle changes through discrete stages and how different myogenic TFs require cooperativity to execute various stage-specific transitions.

Intriguingly, the different stages of healing and changes in chromatin landscape were orchestrated only when binding of small sets of lineage-specific TFs[49] that co-localized and cooperated (or antagonized) with other TFs[50] occurred. An example of this titration of stage-specific transitions was observed between 24h-72h post-injury, whereby temporal increases in members of the IGF and PI3K pathway acted to induce MyoD binding and myogenic transcription but were mediated by MG53, which augments insulin signaling, and XBP1, USF1 NFATc1 and HDACs, which compete for E-box binding with MyoD and MEF2 proteins. This binding pattern uniquely suggests that one or several of these TFs may act as scaffolds to cooperatively recruit various other TFs and chromatin remodeling complexes to enhancers and tune expression. Cooperative or antagonistic binding of TFs during different stages of healing may thus provide an effective means of reinforcing or tuning expression patterns[51] and facilitate a metabolically efficient mechanism to quickly respond after injury. Since muscle repair and

regeneration utilizes many feed-forward and feedback loops, co-occupancy or competition for binding at different *cis* elements by diverse TFs may also facilitate a precise way to prevent extrinsic signal propagation from adjacent tissues that are also regenerating or responding to the injury and rapidly adjust to various changes in metabolic flow.

The temporal events of inflammation, regeneration and muscle differentiation are also fully recapitulated at miRNA levels. Disruption of the muscle integrity stimulated by acute trauma produced miRNA dynamics very similar to those observed in other muscle myophathies, suggesting the modulation of common molecular pathways[46,52].

In summary, this study represents one of the first studies to monitor the in-vivo dynamics of muscle regeneration at genome-wide levels. The simultaneous measurement of epigenetic marks and RNA sequencing including coding and noncoding RNA recapitulated some of the newest players in muscle biology and allowed unbiased views of the actions of various TFs on their targets. We envision that a wider combinatorial interrogation of such a dataset can represent a valuable resource to extend the networks acting in such a complex micro-environment like the cis-regulatory modules engaged by TF, miRNAs and lincRNAs.

Materials and Methods

Animals & Traumatic Injury Model.

Male C57BL/6J mice (10 weeks of age, 24-27 grams) were obtained from The Jackson Laboratory (Bar Harbor, ME). Mice were housed one per cage (shoebox cage, 7" x 11" x 5"h) in the USARIEM animal facility at a constant Ta = 24 ± 1ºC, 50 % relative humidity, with a 12h/ 12h (0600-1800 h) light/dark cycle. Standard laboratory rodent chow and water were provided *ad libitum*. Cages were supplied with Alpha-dri and cob blend bedding for nesting and enrichment and plastic houses for warmth and comfort. Food intake and body mass were recorded daily. Mice were cared for in accordance with the Guide for the Care and Use of Laboratory Animals in a facility accredited by the Association for the Assessment and Accreditation of Laboratory Animal Care (AAALAC).

Prior to administration of the freeze injury, mice were anesthetized with a combination of fentanyl (0.33 mg/kg), droperidol (16.7mg/kg), and diazepam (5 mg/kg). The TA muscle was exposed via a 1 cm long incision in the aseptically prepared skin overlying the TA muscle. Freeze injury was performed in the left, hind limb. The non-injured contralateral leg served as one control. Freeze injury was induced by applying a 6 mm diameter steel probe (cooled to the temperature of dry ice, -70C) to the belly of the TA muscle (directly below incision site) for 10 seconds. Following injury, the skin incision was closed using 6-0 plain gut absorbable suture (Ethicon, Piscataway, NJ). The analgesic, Buprenorphine (0.1 mg/kg SQ) was administered using a 25-27 gauge needle prior to recovery from anesthesia.

Mice were euthanized at each time-point post-injury (3, 10, 24, 48, 72, 168, 336, 504, 672 h) via CO_2 inhalation (2 liters/min), thoracotomy and exsanguination. TA muscles were removed from the injured and contralateral limb; weighed, and a portion of the tissue was crosslinked in 1% formaldehyde for 15 min at room temperature, with constant agitation. The reaction was then quenched with 125mM Glycine for 5 min at room temperature with constant agitation. The fixed tissue was then rinsed 3x with cold PBS (4ºC), spun down, snap frozen in liquid nitrogen and stored for future use.

Chromatin Isolation and Sequencing Library Preparation.

Each frozen tissue was thawed for at least 30 min, homogenized (Tissue Ruptor, Qiagen) and the cells were lysed for at least 10 min. Next, nuclei were isolated, re-suspended and lysed for at least 10 min. The chromatin was then sheared using a Branson sonifier into fragments of size range of 150-700 base-pairs. The sheared chromatin was then incubated overnight at 4ºC with validated antibodies (Modified Histone Peptide Array – Active Motif) H3K4me3 – Millipore Catalog # 07-743, H3K27ac – Active Motif Catalog # 39133, H3K4me1 – Abcam Catalog # ab8895) using constant agitation and co-immunoprecipitated using a mixture of Protein A & Protein G Dynabeads (Life Technologies) for 2 hrs at 4ºC with constant agitation. The immunoprecipitated chromatin was then washed, cross-links reversed and treated with Proteinase K and DNA was purified. Approximately 10ng of isolated DNA was end-repaired (End-It DNA End-Repair Kit, Epicenter), extended and A-tailed (New England Biolabs), and ligated to sequencing adaptor oligos (Illumina). The adaptor-modified library was then amplified by PFU Ultra II Hotstart Master Mix (Agilent) and size-selected to a range of 300-600 base-pairs prior to sequencing. Libraries were pooled and sequenced using an Illumina Genome Analyzer IIx using 44 base-pair single end reads to achieve approximately 20 million aligned reads per sample.

Quantitative PCR and Small-RNA Sequencing Library Preparation.

A portion of the extracted tissue was snap frozen in Trizol and total RNA was isolated from the tissue after homogenization using the miRNeasy Mini Kit (Qiagen) as per the manufacturer's instructions. RNA concentration and integrity were measured with a Nanodrop spectrophotometer (Nanodrop 2000c) and Bioanalyzer (Agilent 2100). If a sample did not pass quality metrics for further processing (RIN>7), the samples were omitted from further processing. mRNA was isolated from the extracted tissues using oligo(dT) Dynabeads (Life Technologies) and reverse transcribed to cDNA using the high Capacity cDNA Reverse Transcription kit (Catalog # 4374966; Life Technologies, Carlsbad, CA). TaqMan MicroRNA Reverse Transcription Kit (Catalog # 4366596) was used to generate template for microRNA quantitative PCR. Quantitative PCR was performed using conditions described previously[34] using the comparative dCt method. Primers/probes used in real-time PCR are shown in Supp. Table 1.

At least 500 ng of isolated total RNA was used to produce small-RNA sequencing libraries. Libraries were prepared according to the specifications of the Truseq smallRNA kit (Illumina) and sequenced on a MiSeq single ended 35bp run (Illumina). A custom program was used to match the FASTQ sequences to the microRNA database (miRBase, www.mirbase.org) for the mouse species (mm9). The program counts exact matches and matches with 17+ base identities with two or fewer mismatches as reads. The program then tallies the reads for each miRNA detected and DESeq was used to normalize the miRNA counts. Heatmap.2 (R language; gplots module) was used to create the heatmap. 841 miRNAs were detected with RPKM>1 for at least one time point and 143 miRNAs showed dynamic behavior (RPKM>100 for at least one time point and fold change >3 compared to uninjured controls).

ChIP-Seq Data Processing.

Individual replicates were aligned to the mm9 mouse genome using Bowtie2[53]. Replicates for a single mark at a single timepoint were merged with the samtools[54] cat command. MACS2[55] was used to call peaks for individual replicates (versus the merged controls for a given timepoint) as well as for the merged datasets (versus the merged controls for a given timepoint). The fold change parameter in MACS2 was set to the [2,500] range, and the –broadpeaks option was

utilized to call peaks for the K4me1 datasets. The –to-large parameter was used to scale the smaller dataset to the larger dataset and the extension size was set to 200 for the K4me1 datasets.

The standard workflow for the IDR framework[56] was used to identify irreproducible peaks from individual replicates: any peaks that were not present in the majority of replicates were excluded from the set of peaks identified by MACS2 for the merged datasets. The peaks that remained after the IDR filtering were analyzed with the GREAT toolkit[57] for the mm9 genome to identify genes and pathways associated with the enriched sites. The gene regulatory domain definition was used to set the association rules. For the K4me3 marks, the GREAT association rules were set to analyze proximal regions 1.5 kbp upstream, 1.5 kbp downstream, and distal 1.5 kbp. For the remaining two marks, the association rules were set to analyze proximal regions 5.0 kbp upstream, downstream, and distally. The MSigDB pathways identified by GREAT with FDR <0.05, using the Bonferroni correction, were selected. Pathways with significant FDR values at 8 timepoints for K27ac, 7 timepoints for K4me3, and 5 timepoints for K4me1 were identified, and significance levels were plotted over time.

In a parallel analysis, the post-IDR peaks from the merged replicates were compared to the genes.gtf file for mm9. Peaks were mapped to promoter regions (within 1.5 kbp of the TSS), the first exon, subsequent exons, and introns, as determined from the exons.gtf file. Peaks were additionally mapped to the near-gene region, defined as within 5 kbp upstream of the TSS or 5 kbp downstream from the final exon. Remaining peaks were assigned to the intergenic region.

The HOMER software suite[58] was used to discover known and *de novo* motifs for the K27ac, K4me3, and K4me1 datasets. The findMotifsGenome.pl tool within the HOMER toolkit was used with the mm9 reference genome, and a threshold of 1e-50 was used to determine result significance for de novo motif discovery.

The final set of peaks from the merged datasets were compared against the MyoD ChIP-Seq datasets from Cao et al[14] (GSM857390, GSM857391) as well as a MyoG ChIP-Seq dataset from Wold et al[15] (ENCFF001XVD). The bedtools intersection tool was used to identify overlapping peaks across these datasets and the datasets generated as part of this study. Upregulated promoter regions were confirmed by analyzing the overlap between the Myod/Myog datasets and the K4me3 dataset. The K4me3 dataset was then compared against the K27ac and K4me1 datasets to identify and remove common peaks, leaving only K27ac and K4me1 peaks that map to enhancer regions. These remaining peaks were subsequently also overlapped with the MyoD/MyoG datasets to confirm upregulated enhancer regions.

The KEGG and GO[59] database was queried to identify pathways that were over-expressed in the injured samples. Additionally, Gene Set Enrichment Analysis[60] using the MsigDB v. 4.0 was performed to identify differentially enriched gene sets. Using the Cytoscape data visualization software[61], upregulated immune response pathways and gene sets (cytokine-cytokine receptor inteaction, chemokine signaling pathways, leukocyte transendothelial migration, genes involved in platelet activation and signal aggregation, Jak-Stat signaling network, AP-1 transcription factor network, genes involved in signaling by interleukins, Il8-and Cxcr2-mediated signaling events, HIF-1-alpha transcription network, TNF receptor signaling pathway, apoptosis, NF-kB signaling pathway) and GPCR signaling pathways were merged to construct interaction networks for upregulated genes in the datasets. All member genes in these pathways that were upregulated with a fold change of two or greater for at least one timepoint were included in the interaction

network. Gene nodes were ranked by out-degree, the number of other genes in the network that the given gene interacts with[62].

Data Visualization

The IGV browser (v.2.3.36)[63] was used to visualize pileup data and to generate the tracks in Figures 1-5. All chromatin maps were converted and visualized as bigWig files normalized to 10M reads. The violin plots in Supplemental Figure 1 were generated with MATLAB's violin function. The ggplots heatmap2 function in R was used to generate all heatmaps.

Acknowledgments

The authors thank Chet Beal for assistance with artwork, Sara Chauvin, Patrick Boyle and Fontina Kelley and the Broad Institute Genomics Platform for sequencing and technical assistance, Tara Boettcher for assistance with ChIP and sequencing library preparation, Mary Abdalla and Alyssa Geddis for technical assistance with PCR, and Eric T. Wang and Michael J. Ziller for insightful discussions. This work is sponsored by the Department of the Air Force under Air Force Contract #FA8721-05-C-0002. Opinions, interpretations, recommendations and conclusions are those of the authors and are not necessarily endorsed by the United States Government. C.C. was supported by an appointment to the postgraduate research participation program at the US Army Research Institute of Environmental Medicine, administered by the Oak Ridge Institute for Science and Education through an interagency agreement between the US Department of Energy and the US Army Medical Research and Materiel Command. The views, opinions, and/or findings of this report are those of the authors and should not be construed as an official US Department of the Army position, policy, or decision unless so designated by other official documentation.

Author contributions

C.A.A., M.L.U. and A.M. conceived the study, C.A.A., M.L.U., R.P., D.C., C.T.C., C.A.G., M.A.K., R.W.M. performed experiments, C.A.A., and A.S. performed computational analysis of the data, A.M. supervised the project, C.A.A. wrote the paper with assistance from the other authors.

Competing interests

The authors declare no competing financial interests.

Figures and Tables

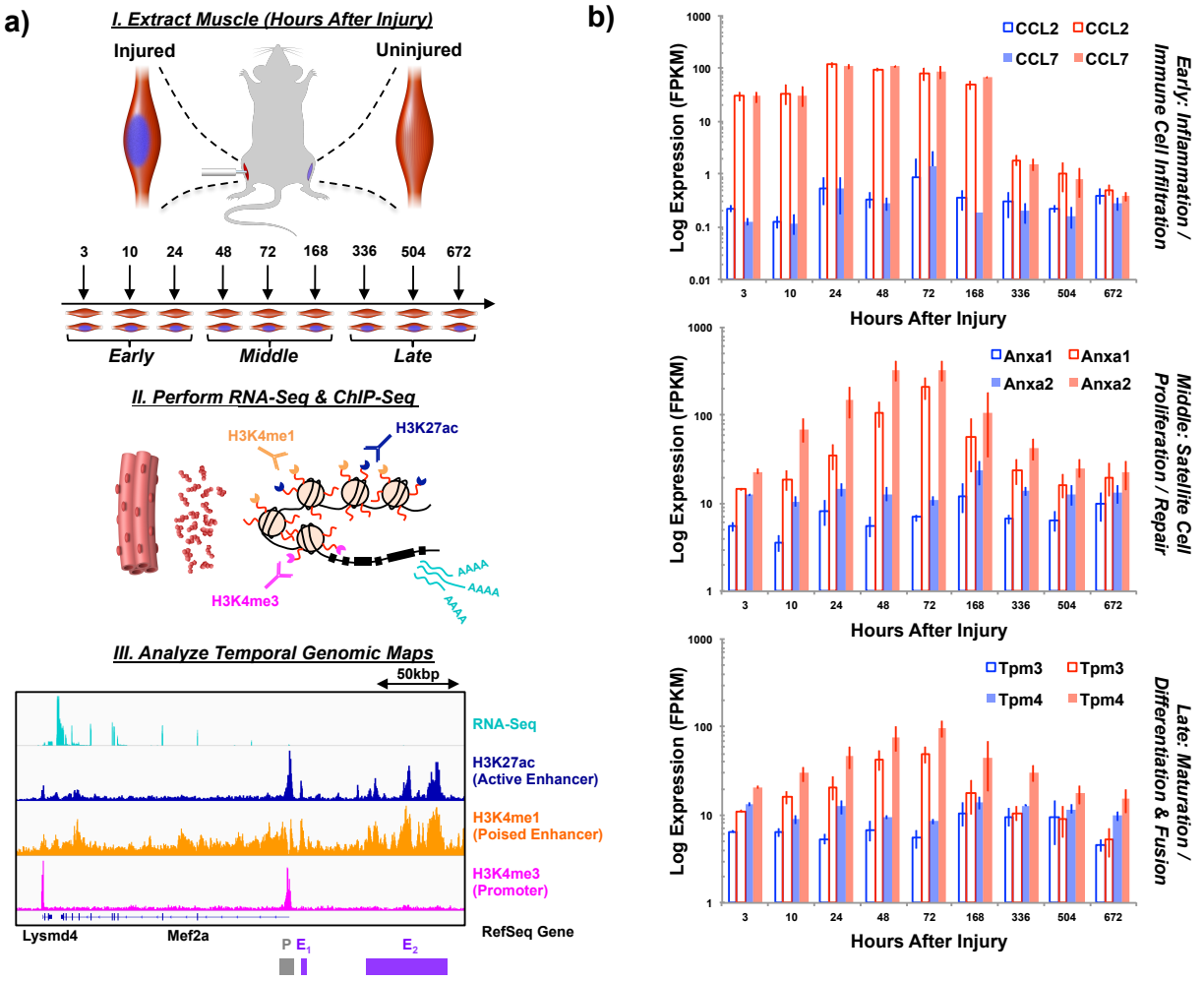

Figure 1. Experimental overview for profiling molecular mechanisms governing *in-vivo* tibialis anterior (TA) muscle regeneration after severe trauma. a) Schematic diagram of injury model and process flow for chromatin and mRNA extraction and analysis of genomic maps. In I, the TA muscle of a C57BL/6J mouse is administered a freeze injury and the contralateral TA muscle serves as the control. The injured and uninjured tissues are extracted at different times after the injury was administered (3hrs-672 hrs). During II, the tissue is digested and mRNA and chromatin are extracted and enriched. In III, the enriched nucleic acids are then sequenced, aligned to the mm9 genome and analyzed. A representative example of the Mef2a gene at 3 hours post-injury is shown where the promoter (labeled P in gray) and enhancer regions (labeled E1 and E2 in purple) are depicted. b) Bar graphs of gene expression values of six different genes corresponding to different stages of the muscle regeneration process through time from left to right.

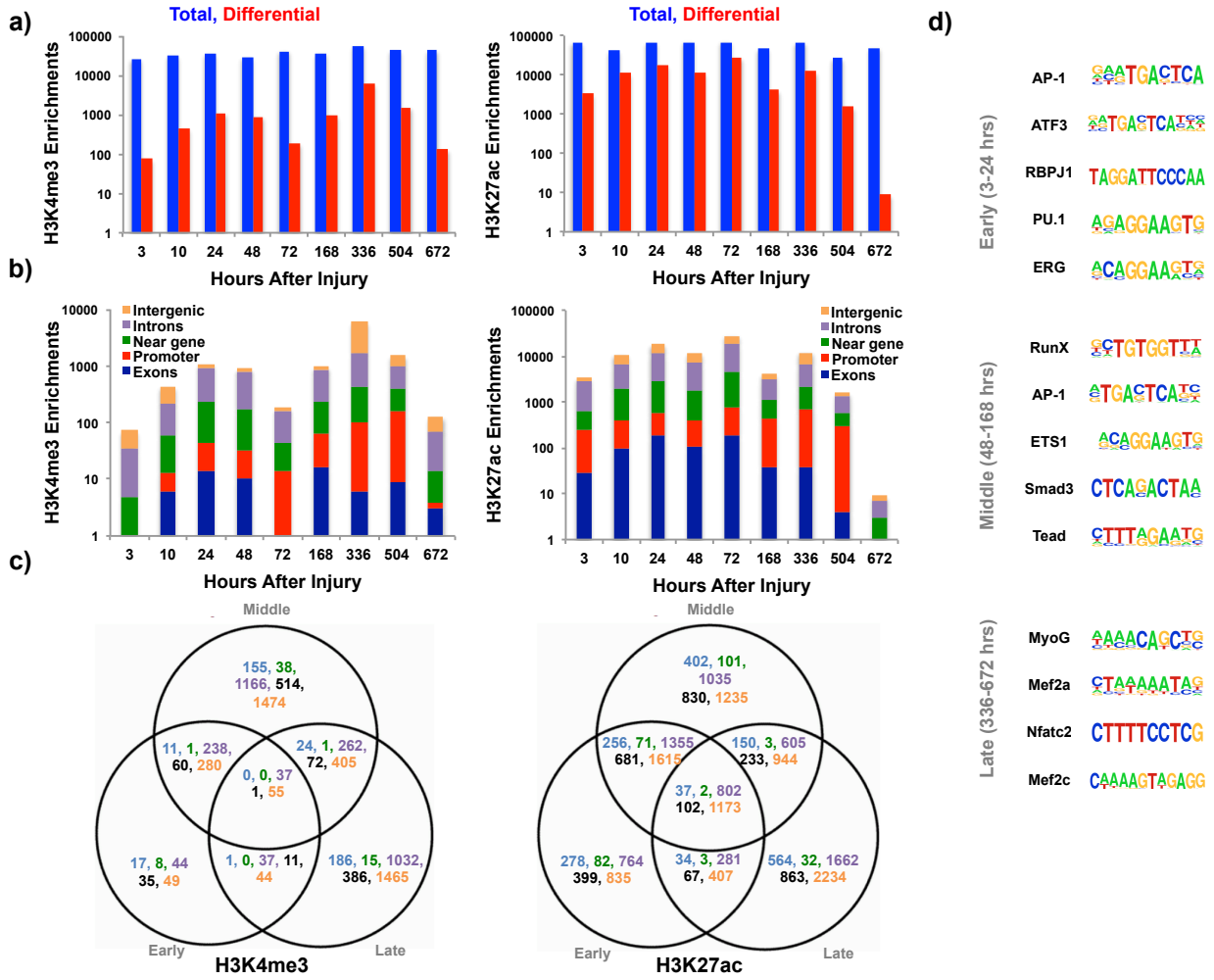

Figure 2. Distribution of enriched sites across the genome during *in-vivo* muscle regeneration. a) Total and differential number of enriched sites for H3K27ac and H3K4me3. b) Distribution of peaks across various genomic elements (promoter, intergenic, intron, near-gene: ± 2kbp from transcriptional start site, exon). c) Shared and unique numbers of enriched chromatin sites corresponding to different genomic elements in b). d) Representative motifs of overrepresented transcription factors ($p < 10^{-10}$) enriched from H3K27ac and H3K4me1-marked regions for the different stages (early, middle and late).

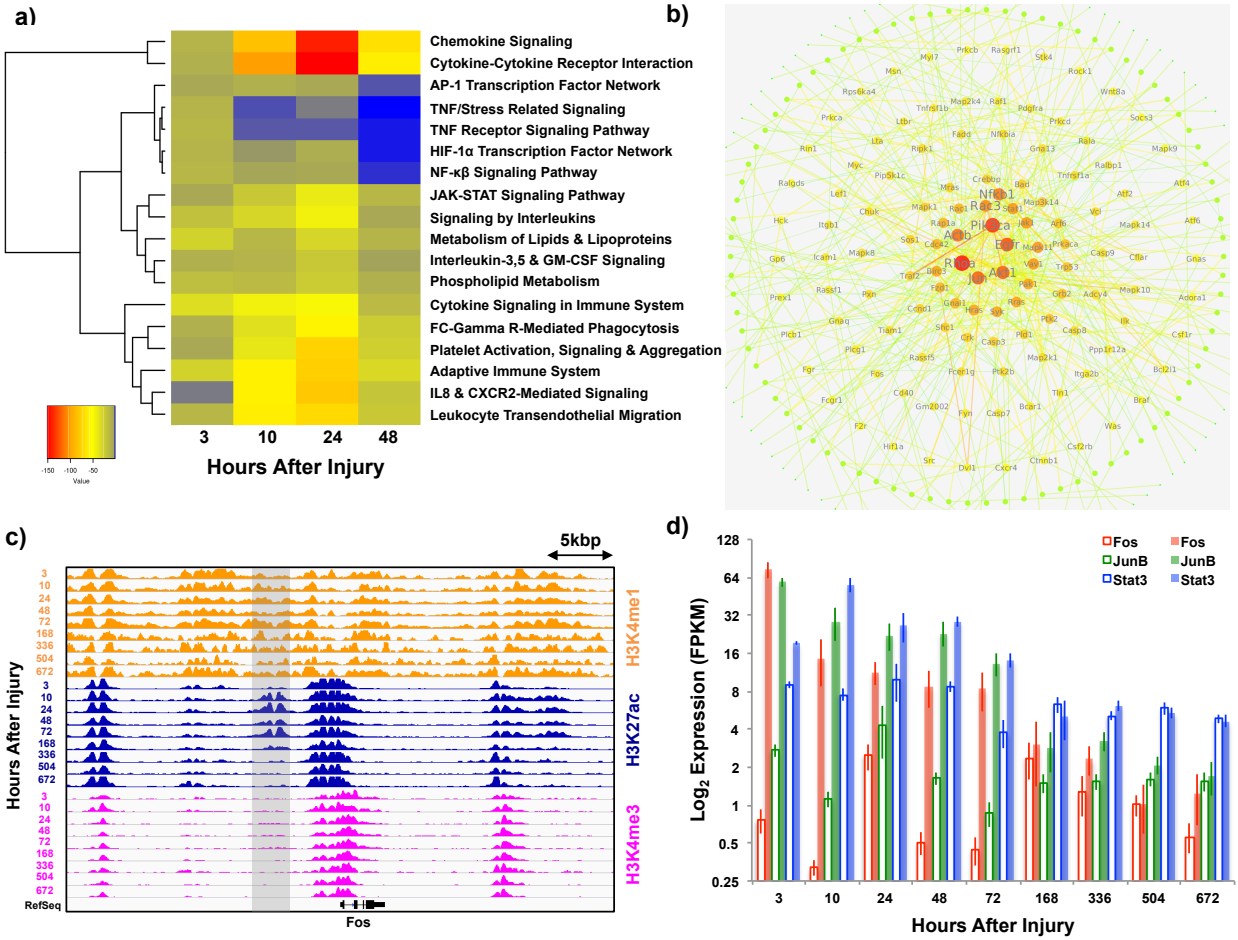

Figure 3. Chromatin landscapes are immediately modified after severe muscle trauma and reflect immune cell infiltration. a) Heatmap of overrepresented immune system pathways derived from enriched H3K27ac peaks. b) Interaction network diagram of upregulated gene sets derived from over-represented pathways in the early period. c) Normalized H3K4me1, H3K27ac, and H3K4me3 ChIP-Seq profiles of peaks found around the c-Fos locus. Enriched enhancer regions are highlighted in gray. d) Bar graphs of individual gene expression values of four regulator genes through time from left to right (injured samples are colored and uninjured samples are uncolored).

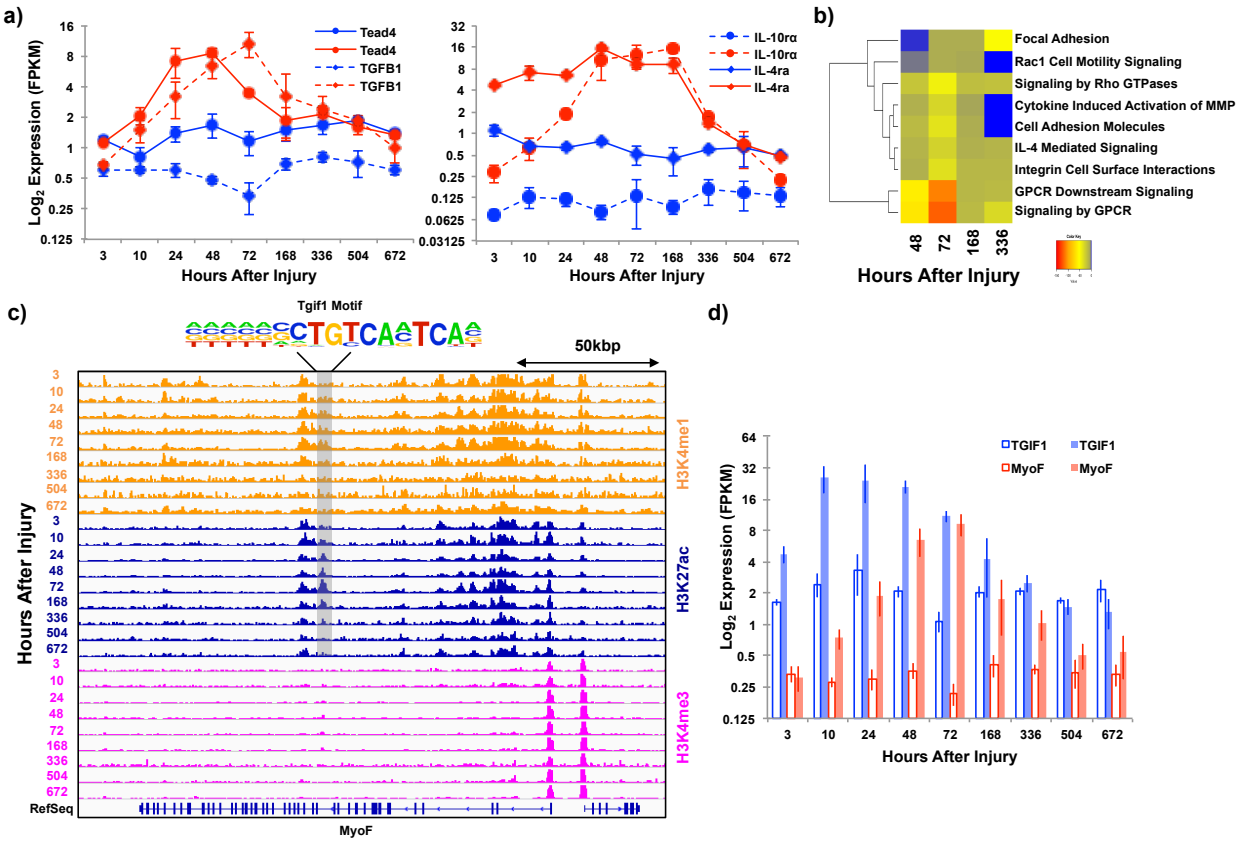

Figure 4. Injured muscle microenvironment provides cues for chromatin remodeling at genes associated with satellite cell migration and proliferation. a) Line graphs of individual gene expression values through time from left to right of SMAD-activated genes (TGF-β1 and Tead4) that promote TGF-β signaling and a transition towards Hippo and Wnt signaling. Serum response factor (SRF) targets interleukin-4 (IL-4ra) and interleukin-10 (IL-10ra) also show upregulation at this time, which induce macrophage M2 polarization and modulate MyoD expression. b) Heatmap of overrepresented pathways corresponding to G-protein coupled receptors and Rho family of small GTPases, which were derived from enriched H3K27ac peaks. c) Normalized ChIP-Seq tracks of H3K4me1, H3K27ac, and H3K4me3 profiles around the myoferlin (MyoF) gene, a plasma membrane protein. Enriched enhancer regions are highlighted in gray and corresponding enriched TF motif is labeled. d) Bar graphs of individual gene expression values of MyoF and associated transcription factor (TGIF1) through time from left to right (injured samples are colored and uninjured samples are uncolored).

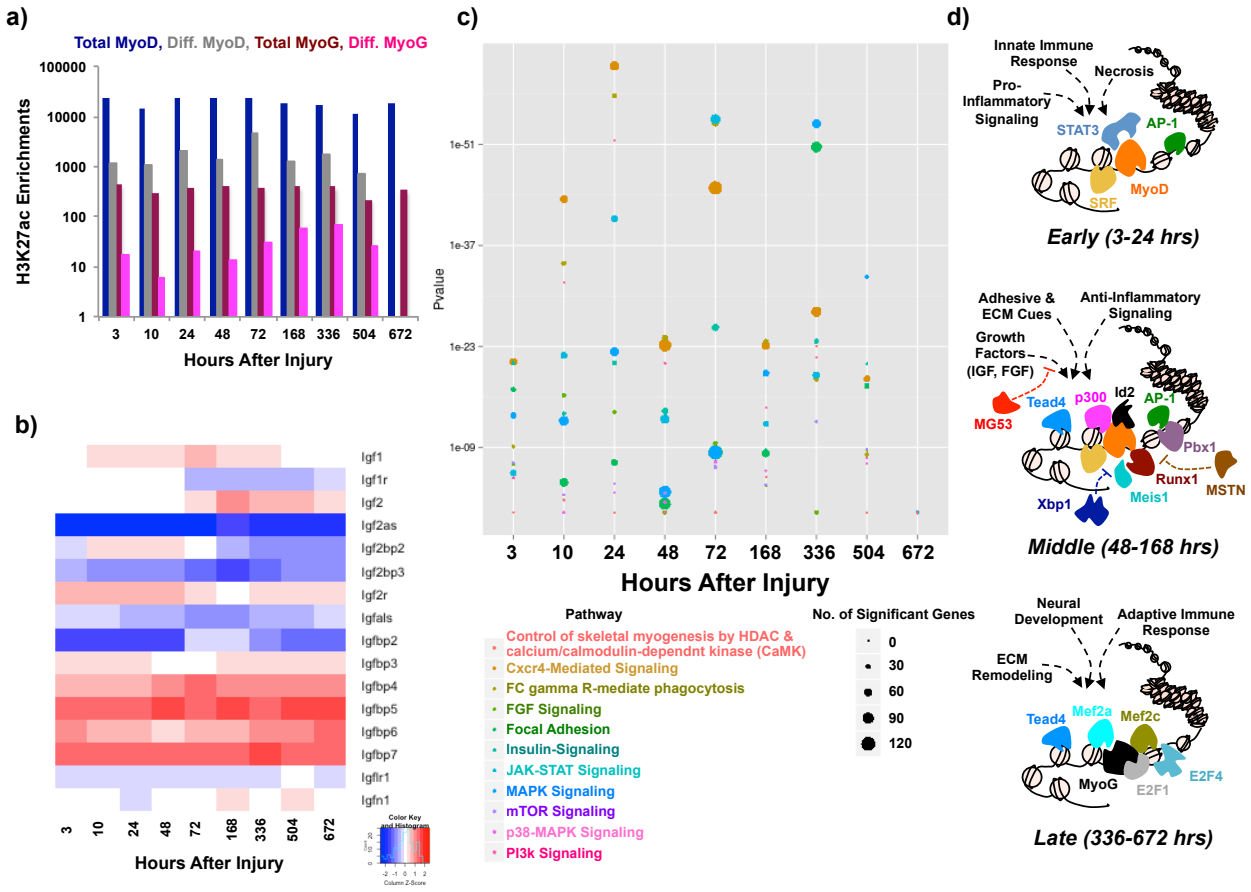

Figure 5. Coordinated activation of myogenic differentiation and healing. a) Analysis of total and differential activity at enhancers for MyoD and MyoG derived from H3K27ac^{+} & H3K4me3^{-} sites. b) Expression heatmap of IGF signaling genes through time from left to right. c) Enriched GO terms derived from differential chromatin peaks at enhancer elements show associations with myogenic differentiation. The corresponding false discovery rates for different times after injury are plotted and the size of each circle corresponds to the number of significant genes associated with the category (insulin growth factor: IGF, fibroblast growth factor: FGF, p38 mitogen-activated protein kinase: p38-MAPK, phosphatidylinositol 3-kinase: PI3K). d) Proposed integrated model of detected transcription factors (TFs) associated with enhancer elements at different stages after injury.

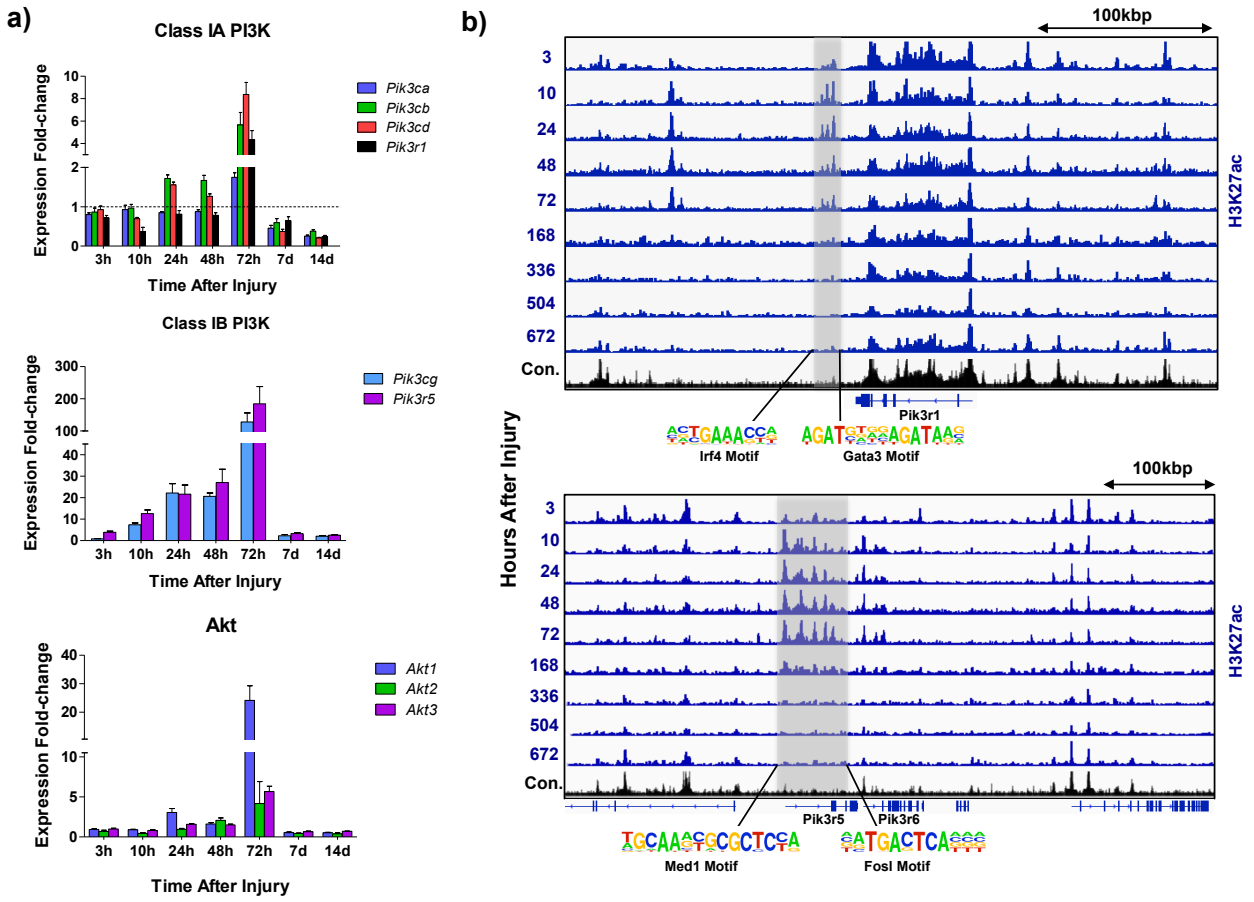

Figure 6. PI3K/Akt activation promotes transition from proliferation towards myogenic differentiation. a) Bar graphs of individual gene expression values for various components of the PI3K and AKT pathways through time from left to right. b) Normalized ChIP-Seq tracks of H3K27ac profiles showing differential enhancer activity of the PI3Kr1, PI3Kr5 and PI3Kr6 loci. Enriched enhancer regions are highlighted in gray and corresponding enriched TF motifs are labeled underneath.

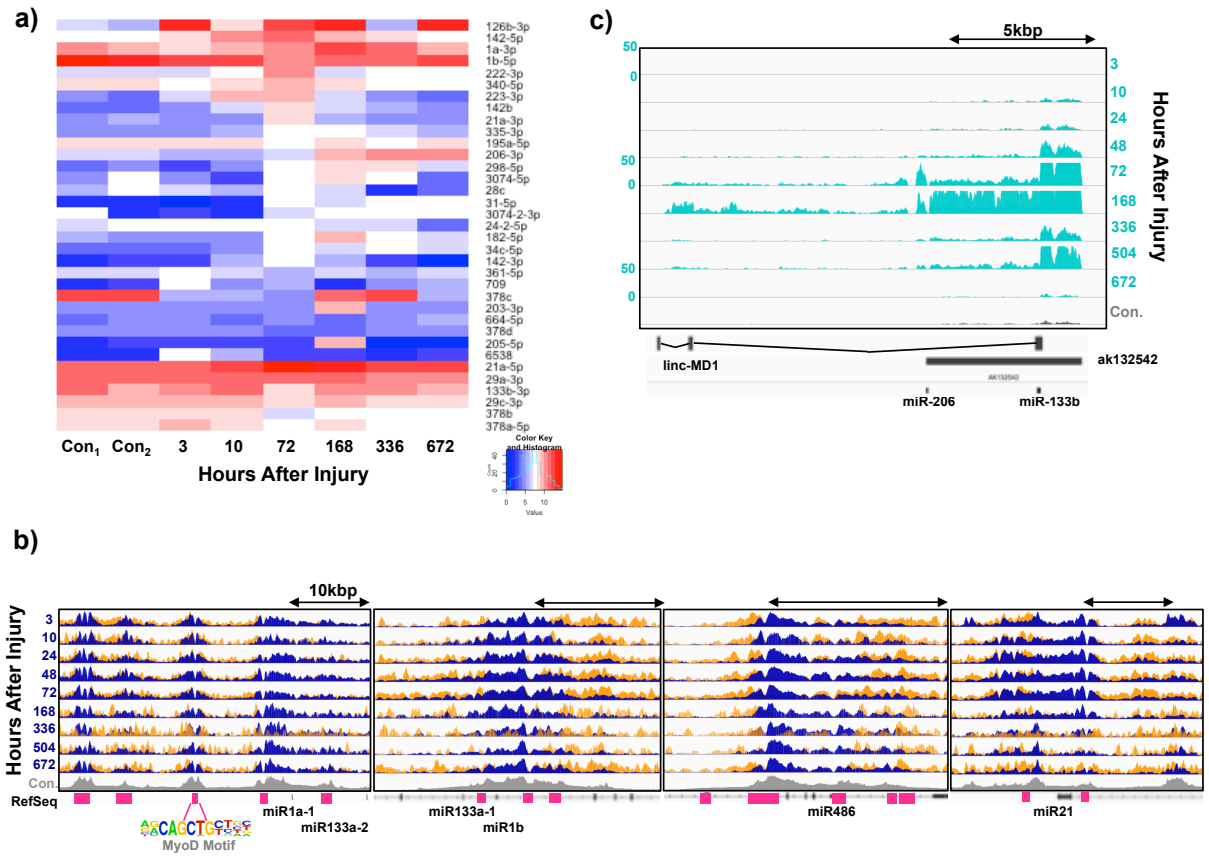

Figure 7. Dynamics of non-coding RNAs after severe muscle trauma. a) Expression heatmap for small RNAs are plotted through time from left to right. Muscle-specific miRNAs and miRNAs with dynamic expression exhibited temporal events of inflammation, repair and regeneration. Early upregulated microRNAs were associated with inflammation and immune system programs (miR-223) and middle and late upregulated microRNA genes were correlated with muscle repair and regeneration (miR-126b, miR-29, miR-21, miR-31, miR-378). b) Chromatin profiles of several microRNA genes for two histone modifications (H3K27ac-blue and H3K4me1-orange) associated with enhancer elements. The maps are ordered through time and MyoD enrichments from Cao et al[14] are labeled underneath the track with a pink box. Each scale bar is 10 kbp. c) Expression profile of the linc-MD1 gene, which sequesters microRNAs that inhibit transcriptional programs such as myogenic differentiation. The expression of linc-MD1 increased at 72h and peaked at 168h, which was consistent with the peak times observed for myoblast proliferation and onset of differentiation.

References

1. Scharner, J. and Zammit, P.S. The muscle satellite cell at 50: the formative years. *Skelet. Muscle* **1**, 28 (2011).
2. Bentzinger, C.F., Wang, Y.X., Dumont, N.A., and Rudnicki, M.A. Cellular dynamics in the muscle satellite cell niche. *EMBO Rep.* **14**, 1062-1072 (2013).
3. Kuang, S., Gillespie, M.A., Rudnicki, M.A. Niche regulation of muscle satellite cell self-renewal and differentiation. *Cell Stem Cell* **2**, 22-31 (2008).
4. Aurora, A.B. and Olson, E.N. Immune modulation of stem cells and regeneration. *Cell Stem Cell* **15**, 14-25 (2014).
5. Burzyn, D., Kuswanto, W., Kolodin, D., Shadrach, J.L., Cerletti, M., Jang, Y., Sefik, E., Tan, T.G., Wagers, A.J., Benoist, C. and Mathis, D. A special population of regulatory T cells potentiates muscle repair. *Cell* **155**, 1282-1295 (2013).
6. Heredia, J.E., Mukundan, L., Chen, F.M., Mueller, A.A., Deo, R.C., Locksley, R.M., Rando, T.A. and Chawla, A. Type 2 innate signals stiumulate fibro/adipogenic progenitors to facilitate muscle regeneration. *Cell* **153**, 376-388 (2013).
7. Braun, T. and Gautel, M. Transcriptional mechanisms regulating skeletal muscle differentiation, growth and homeostasis. *Nature Rev. Molec. Cell Biol.* **12**, 349-361 (2011).
8. Asp, P., Blum, R., Vethantham, V., Parisi, F., Micsinai, M., Cheng, J., Bowman, C., Kluger, Y., and Dynlacht, B.D. Genome-wide remodeling of the epigenetic landscape during myogenic differentiation. *Proc. Nat'l. Acad. Sci. USA* **108**, E149-E158 (2011).
9. Brancaccio, A., Palacios, D. Chromatin signaling in muscle stem cells: interpreting the regenerative microenvironment. *Front. Aging Neurosci.* **7**, 1-17 (2015).
10. Buckingham, M. and Rigby, P.W.J. Gene regulatory networks and transcriptional mechanisms that control myogenesis. *Devel. Cell* **28**, 225-238 (2014).
11. Roadmap Epigenomics Consortium et al. Integrative analysis of 111 reference human epigenomes. *Nature* **518**, 317-330 (2015).
12. Liu, L., Cheung, T.H., Charville, G.W., Hurgo, B.M.C., Leavitt, T., Shih, J., Brunet, A. and Rando, T.A. Chromatin modifications as determinants of muscle stem cell quiescence and chronological aging. *Cell Rep.* **4**, 189-204 (2013).
13. Giordani, L. and Puri, P.L. Epigenetic control of skeletal muscle regeneration: integrating genetic determinants and environmental changes. *FEBS* **280**, 4014-4025 (2013).
14. Cao, Y., Yao, Z., Sarkar, D., Lawrence, M., Sanchez, G.J., Parker, M.H., MacQuarrie, K.L., Davison, J., Morgan, M.T., Ruzzo, W.L., Gentleman, R.C., Tapscott, S.J. Genome-wide MyoD binding in skeletal muscle cells: a potential for broad cellular reprogramming. *Dev. Cell* **18**, 662-674 (2010).
15. The Mouse ENCODE consortium. A comparative encyclopedia of DNA elements in the mouse genome. *Nature* **515**, 355-364 (2014).
16. Ernst, J., Kheradpour, P., Mikkelsen, T.S., Shoresh, N., Ward, L.D., Epstein, C.B., Zhang, X., Wang, L., Issner, R., Coyne, M., Ku, M., Durham, T., Kellis, M. and Bernstein, B.E. Mapping and analysis of chromatin state dynamics in nine human cell types. *Nature* **473**, 43-49 (2011).
17. Aguilar, C.A., Shcherbina, A., Ricke, D.O., Pop, R., Carrigan, C.T., Gifford, C.A., Urso, M.L., Kottke, M.A., and Meissner, A. In vivo monitoring of transcriptional dynamics after lower-limb muscle injury enables quantitative classification of healing. *Sci. Rep.* **5,** 13885 (2015).

18. Garber, M., Yosef, N., Goren, A., Raychowdhury, R., Thielke, A., Guttman, M., Robinson, J., Minie, B., Chevrier, N., Itzhaki, Z., Blecher-Goren, R., Bonstein, C., Amann-Zalcenstein, D., Weiner, A., Freidrich, D., Medrim, J., Ram, O., Cheng, C., Gnirke, A., Fisher, S., Friedman, N., Wong, B., Bernstein, B.E., Nusbaum, C., Hacohen, N., Regev, A. and Amit, A. A high-throughput chromatin immunoprecipitation approach reveals principles of dynamic gene regulation in mammals. *Molec. Cell* **47**, 1-13 (2012).
19. Rada-Iglesias, A., Bajpai, R., Swigut, T., Brugmann, S.A., Flynn, R.A., and Wysocka, J. A unique chromatin signature uncovers early developmental enhancers in humans. *Nature* **470**, 279–283 (2011).
20. Creyghton, M.P., Cheng, A.W., Welstead, G.G., Kooistra, T., Carey, B.W., Steine, E.J., Hanna, J., Lodato, M.A., Frampton, G.M., Sharp, P.A., Boyer, L.A., Young, R.A. and Jaenisch,. R. Histone H3K27ac separates active from poised enhancers and predicts developmental state. *Proc. Nat'l. Acad. Sci. USA* **107**, 21931-21936 (2010).
21. Toth, K.G., McKay, B.R., De Lisio, M., Little, J.P., Tarnopolsky, M.A., Parise, G. IL-6 induced Stat3 signalling is associated with the proliferation of human muscle satellite cells following acute muscle damage. *PLOS One* **6**, e17392 (2011).
22. Brack, A.S., Conboy, I.M., Conboy, M.J., Shen, J., and Rando, T.A. A Temporal Switch from Notch to Wnt Signaling in Muscle Stem Cells Is Necessary for Normal Adult Myogenesis. *Cell Stem Cell* **2**, 50-59 (2009).
23. Wackerhage, H., Del Re, D.P., Judson, R.N., Sudol, M., Sadoshima, J. The Hippo signal transduction network in skeletal and cardiac muscle. *Science Sign.* **7**, re4 (2014).
24. Carnac, G., Primig, M., Kitzmann, M., Chafey, P., Tuil, D., Lamb, N., Fernandez, A. RhoA GTPase and serum response factor control selectively the expression of MyoD without affecting Myf5 in mouse myoblats. *Mol. Biol. Cell* **9**, 1891-1902 (1998).
25. Engler, A.J., Griffin, M.A., Sen, S., Bonnemann, C.G., Sweeney, H.L., and Discher, D.E. Myotubes differentiate optimally on substrates with tissue-like stiffness: pathological implications for soft or stiff microenvironments. *J. Cell Biol.* 166, 877–887 (2004).
26. Judson, R.N., Tremblay, A.M., Knopp, P., White, R.B., Urcia, R., De Bari, C., Zammit, P.S., Camargo, F.D. and Wackerhage, H. The Hippo pathway member Yap plays a key role in influencing fate decisions in muscle satellite cells. *J. Cell Sci.* **125**, 6009-6019 (2012).
27. McKinsey, T.A., Zhang, C.L., Lu, J., Olson, E.N. Signal-dependent nuclear export of a histone deacetylase regulates muscle differentiation. *Nature* **408**, 106-111 (2000).
28. Gilbert, P.M., Havenstrite, K.L., Magnusson, K.E.G., Sacco, A., Leonardi, N.A., Kraft, P., Nguyen, N.K., Thrun, S., Lutolf, M.P., Blau, H.M. Substrate elasticity regulates skeletal muscle stem cell self-renewal in culture. *Science* **329**, 1078-1081 (2010).
29. Ostuni, R., Piccolo, V., Barozzi, I., Polletti, S., Termanini, A., Bonifacio, S., Curina, A., Prosperini, E., Ghisletti, S. and Natoli, G. Latent enhancers activated by stimulation in differentiated cells. *Cell* **152**, 157-171 (2013).
30. Maves, L., Waskiewicz, A.J., Paul, B., Cao, Y., Tyler, A., Moens, C.B., Tapscott, S.J. Pbx homeodomain proteins direct Myod activity to promote fast-muscle differentiation. *Develop.* **134**, 3371-3382 (2007).
31. Schiaffino, S., Mammucari, C. Regulation of skeletal muscle growth by the IGF1-Akt/PKB pathway: insights from genetic models. *Skele. Musc.* **1**, 1-14 (2011).
32. Keren, A., Tamir, Y., Bengal, E. The p38 MAPK signaling pathway: a major regulator of skeletal muscle development. *Molec. Cell. Endocrin.* **252**, 224-230 (2006).

33. Joe, A.W.B., Yi, L., Natarajan, A., Le Grand, F., So, L., Wang, J., Rudnicki, M.A., and Rossi, F.M.V. Muscle injury activates resident fibro/adipogenic progenitors that facilitate myogenesis. *Nature Cell Biol.* **12**, 153-163 (2010).
34. Matheny, R.W., and Adamo, M.L. PI3K p110 alpha and p110 beta have differential effects on Akt activation and protection against oxidative stress-induced apoptosis in myoblasts. *Cell Death Differ.* **17**, 677-688 (2010).
35. Matheny, R.W., Riddle-Kottke, M.A., Leandry, L.A., Lynch, C.M., Abdalla, M.N., Geddis, A.V., Piper, D.R., and Zhao, J.J. Role of phosphoinositide 3-OH kinase p110beta in skeletal myogenesis. *Mol. Cell Biol.* **35**, 1182-1196 (2015).
36. Matheny, R.W., Lynch, C.M., and Leandry LA. Enhanced Akt phosphorylation and myogenic differentiation in PI3K p110beta-deficient myoblasts is mediated by PI3K p110alpha and mTORC2. *Growth Factors* **30**, 367-384 (2012).
37. Yi, J.S., Park, J.S., Ham, Y.M., Nguyen, N., Lee, N.R., Hong, J., Kim, B.W., Lee, H., Lee, C.S., Jeong, B.C., Song, H.K., Cho, H., Kim, Y.K., Lee, J.S., Park, K.S., Shin, H., Choi, I., Lee, S.H., Park, W.J., Park, S.Y., Choi, C.S., Lin, P., Karunasiri, M., Tan, T., Duann, P., Zhu, H., Ma, J. and Ko, Y.G. MG53-induced IRS-1 ubiquitination negatively regulates skeletal myogenesis and insulin signalling. *Nature Commun.* **4**:2354 (2013).
38. Acosta-Alvear, D., Zhou, Y., Blais, A., Tsikitis, M., Lents, N.H., Arias, C., Lennon, C.J., Kluger, Y., and Dynlacht, B.D. XBP1 controls diverse cell type- and condition-specific transcriptional regulatory networks. *Mol. Cell* **27,** 53-66 (2007).
39. Ehlers, M.L., Celona, B., Black, B.L. NFATc1 controls skeletal muscle fiber type and is a negative regulator of MyoD activity. *Cell Rep.* **8,** 1639-1648 (2014).
40. Puri, P.L., Iezzi, S., Stiegler, P., Chen, T.T., Schiltz, R.L., Muscat, G.E.O., Giodano, A., Kedes, L., Wang, J.Y.J., Sartorelli, V. Class I histone deacetylases sequentially interact with MyoD and pRb during skeletal myogenesis. *Mol. Cell* **8**, 885-897 (2001).
41. Chen, J.F., Mandel, E.M., Thomson, J.M., Wu, Q., Callis, T.E., Hammond, S.M., Conlon, F.L., and Wang, D.Z. The role of microRNA-1 and microRNA-133 in skeletal muscle proliferation and differentiation. *Nature Genet.* **38**, 228-233 (2005).
42. Kim, H.K., Lee, Y.S., Sivaprasad, U., Malhotra, A., Dutta, A. Muscle specific microRNA miR-206 promotes muscle differentiation. *J. Cell Biol.* **174**, 677-687 (2006).
43. Rao, P.K., Kumar, R.M., Farkhondeh, M., Baskerville, S., and Lodish, H.F. Myogenic factors that regulate expression of muscle-specific microRNAs. *Proc. Nat'l. Acad. Sci. USA* **103**, 8721-8726 (2006).
44. Zhang, Y., Yang, P., Sun, T., Li, D., Xu, X., Rui, Y., Li, C., Chong, M., Ibrahim, T., Mercatali, L., Amadori, D., Lu, X., Xie, D., Li, Q.J., Wang, X.F. miR-126 and miR-126* repress recruitment of mesenchymal stem cells and inflammatory monocytes to inhibit breast cancer metastasis. *Nature Cell Biol.* **15**, 284-294 (2013).
45. Cachiarelli, D., Incitti, T., Martone, J., Cesana, M., Cazzella, V., Santini, T., Sthandier, O., Bozzoni, I. miR-31 modulates dystrophin expression: new implications for Duchenne muscular dystrophy therapy. *EMBO Rep.* **12**, 136-141 (2011).
46. Cachiarelli, D., Martone, J., Girardi, E., Cesana, M., Incitti, T., Morlando, M., Nicoletti, C., Santini, T., Sthandier, O., Barberi, L., Auricchio, A., Musaro, A., Bozzoni, I. MicroRNAs involved in molecular circuitries relevant for the Duchenne muscular dystrophy pathogenesis are controlled by the dystrophin/nNOS pathway. *Cell Metab.* **12**, 341-351 (2010).

47. Cesana, M., Cacchiarelli, D., Legnini, I., Santini, T., Sthandier, O., Chinappi, M., Tramontano, A., Bozzoni, I. A long noncoding RNA controls muscle differentiation by functioning as a competing endogenous RNA. *Cell* **147**, 358-369 (2011).
48. Palacios, D., and Puri, P.L. The epigenetic network regulating muscle development and regeneration. *J Cell Physiol.* **207**, 1-11 (2006).
49. Blais, A., Tsikitis, M., Acosta-Alvear, D., Sharan, R., Kluger, Y., Dynlacht, B.D. An initial blueprint for myogenic differentiation. *Genes Dev.* **19**, 553–569 (2005).
50. Blum, R., Vethanthum, V., Bowman, C., Rudnicki, M., Dynlacht, B.D. Genome-wide identification of enhancers in skeletal muscle: the role of MyoD1. *Genes Dev.* **26**, 2763-2779 (2012).
51. Tsankov, A.M., Gu, H., Akopian, V., Ziller, M.J., Donaghey, J., Amit, I., Gnirke, A., and Meissner, A. Transcription factor binding dynamics during human ES cell differentiation. *Nature* **518**, 344-349 (2015).
52. Eisenberg, I., Eran, A., Nishino, I., Moggio, M., Lamperti, C., Amato, A.A., Lidov, H.G., Kang, P.B., North, K.N., Mitrani-Rosenbaum, S., Flanigan, K.M., Neely, L.A., Whitney, D., Beggs, A.H., Kohane, I.S., Kunkel, L.M. Distinctive patterns of microRNA expression in primary muscular disorders. *Proc. Nat'l. Acad. Sci. USA* **104**, 17016-17021 (2007).
53. Langmead, B., Salzberg, S. Fast gapped-read alignment with Bowtie 2. *Nature Meth.* **9**, 357-359 (2012).
54. Li, H., Handsaker, B., Wysoker, A., Fennell, T., Ruan, J., Homer, N., Marth, G., Abecassis, G., Durbin, R. The sequence alignment map format and SAM tools. *Bioinf.* 2078-2079 (2009).
55. Zhang, Y., Liu, T., Meyer, C.A., Eeckhoute, J., Johnson, D.J., Bernstein, B.E., Nusbaum, C., Myers, R.M., Brown, R.M., Brown, M., Li, W., Liu, X.S. Model-based Analysis of ChIP-Seq (MACS). *Genome Biol.* **9**, 137 (2008).
56. Li, Q., Brown, J.B., Huang, H., Bickel, P.J. Measuring reproducibility of high-throughput experiments. *Ann. Appl. Stat.* **5**, 1752-1779 (2011).
57. McLean, C.Y., Bristor, D., Hiller, M., Clarke, S.C., Schaar, B.T., Lowe, C.B., Wenger, A.M., Bejerano, G. GREAT improves functional interpretation of *cis*-regulatory regions. *Nature Biotech.* **28**, 495-501 (2010).
58. Heinz, S., Benner, C., Spann, N., Bertolino, E., Lin, Y.C., Laslo, P., Cheng, J.X., Murre, C., Singh, H., Glass, C.K. Simple combinations of lineage determining transcription factors prime *cis*-regulatory elements required for macrophage and B cell identities. *Mol. Cell* **38**, 576–589 (2010).
59. Ashburner, M., Ball, C.A., Blake, J.A., Botstein, D., Butler, H., Cherry, J.M., Davis, A.P., Dolinski, K., Dwight, S.S., Eppig, J.T., Harris, M.A., Hill, D.P., Issel-Tarver, L., Kasarskis, A., Lewis, S., Matese, J.C., Richardson, J.E., Ringwald, M., Rubin, G.M., Sherlock, G. Gene ontology: tool for the unification of biology *Nature Genet.* **25**, 25-29 (2000).
60. Subramanian, A. et al. Gene set enrichment analysis: A knowledge-based approach for interpreting genome-wide expression profiles. *Proc. Nat'l. Acad. Sci. USA* **102**, 15545-15550 (2005).
61. Shannon, P., Markiel, A., Ozier, O., Baliga, N.S., Wang, J.T., Ramage, D., Amin, N., Schwikowski, B., Ideker, T. Cytoscape: a software environment for integrated models of biomolecular interaction networks. *Genome Res.* **13**, 2498-504 (2003).
62. Ogata, H., Goto, S., Sato, K., Fujibuchi, W., Bono, H., Kanehisa, M. KEGG: Kyoto Encyclopedia of Genes and Genomes. *Nucleic Acids Res*. **27**, 29-34.

63. Robinson, J.T., Thorvaldsdóttir, H., Winckler, W., Guttman, M., Lander, E.S., Getz, G., Mesirov, J.P. Integrative Genomics Viewer. *Nature Biotech.* **29**, 24–26 (2011).